TTP96-10
MADPH-96-935
March 1996

Jet Production in Deep Inelastic Scattering at HERA *

Erwin Mirkes[a] and Dieter Zeppenfeld[b]

[a] *Institut für Theoretische Teilchenphysik, Universität Karlsruhe, D-76128 Karlsruhe, Germany*

[b] *Department of Physics, University of Wisconsin, Madison, WI 53706, USA*

Abstract

Two-jet cross sections in deep inelastic scattering at HERA are calculated in next-to-leading order. The importance of higher order corrections and recombination scheme dependencies is studied for various jetalgorithms. Some implications for the determination of $\alpha_s(\mu_R^2)$, the determination of the gluon density and the associated forward jet production in the low x regime at HERA are briefly discussed.

*Invited talk given at the Cracow Epiphany Conference on Proton Structure, Krakow, January 5-6,1996; presented by E. Mirkes

I. INTRODUCTION

Deep inelastic scattering (DIS) at HERA is a copious source of multi-jet events. Typical two-jet cross sections[1] are in the 100 pb to few nb range and thus provide sufficiently high statistics for precision QCD tests [1]. Clearly, next-to-leading order (NLO) QCD corrections are mandatory on the theoretical side for such tests. Full NLO corrections for one and two-jet production cross sections and distributions are now available and implemented in the $ep \to n$ jets event generator MEPJET, which allows to analyze arbitrary jet definition schemes and general cuts in terms of parton 4-momenta [2]. A variety of topics can be studied with these tools. They include

- The determination of $\alpha_s(\mu_R^2)$ over a wide range of scales: The dijet cross section is proportional to $\alpha_s(\mu_R)$ at leading order (LO), thus suggesting a direct measurement of the strong coupling constant. However, the LO calculation leaves the renormalization scale μ_R undetermined. The NLO corrections substantially reduce the renormalization and factorization scale dependencies which are present in the LO calculations and thus reliable cross section predictions in terms of $\alpha_s(m_Z)$ (for a given set of parton distributions) are made possible.

- The measurement of the gluon density in the proton (via $\gamma g \to q\bar{q}$): The gluon density can only be indirectly constrained by an analysis of the structure function F_2 at HERA [3]. The boson gluon fusion subprocess dominates the two jet cross section at low x and allows for a more direct measurement of the gluon density in this regime. A first LO experimental analysis has been presented in [4]. NLO corrections reduce the factorization scale dependence in the LO calculation (due to the intital state collinear factorization, which introduces a mixture of the quark and gluon densities according to the Altarelli-Parisi evolution) and thus reliable cross section predictions in terms of the scale dependent parton distributions are made possible.

- The study of internal jet structure: NLO corrections in jet physics imply that a jet (in a given jet definition scheme) may consist of two partons. Thus first sensitivity to the internal jet structure is obtained, like dependence on the cone size or on recombination prescriptions. These studies are also important for reliable QCD studies (such as the α_s or gluon density determinations). The recombination dependence is only simulated at tree level in the NLO calculation and thus the dependence of the cross section on the recombination scheme is subject to potentially large higher oder corrections.

- Associated forward jet production in the low x regime as a signal of BFKL dynamics: BFKL evolution [5] leads to a larger cross section for events with a measured forward jet (in the proton direction) with transverse momentum $p_T^{lab}(j)$ close to Q than the DGLAP [6] evolution. Clearly, next-to-leading order QCD corrections for fixed order QCD, with Altarelli-Parisi (DGLAP) evolution, are mandatory on the theoretical side in order to establish a signal for BFKL evolution in the data.

---

[1] In the following the jet due to the beam remnant is not included in the number of jets.

- The determination of the polarized gluon structure function (via $\gamma g \to q\bar{q}$) in polarized electron on polarized proton scattering [7]: The measurement of the polarized parton densities and in particular the polarized gluon density from dijet production at a polarized electron proton machine at HERA energies would allow to discriminate between the different pictures of the proton spin underlying these parametrizations. We will analyze these effects in a subsequent publication.

Some theoretical aspects related to these studies are discussed in the following.

II. TECHNICAL MATTERS AND JET ALGORITHMS

The goal of a versatile NLO calculation is to allow for an easy implementation of an arbitrary jet algorithm or to impose any kinematical resolution and acceptance cuts on the final state particles. This is best achieved by performing all hard phase space integrals numerically, with a Monte Carlo integration technique. This approach also allows an investigation of the recombination scheme dependence of the NLO jet cross sections. For dijet production at HERA such a NLO Monte Carlo program is MEPJET.

The basic features of the calculation are described in [2] and we repeat only some of them here. In Born approximation, the subprocesses $\gamma^* + q \to q + g$, $\gamma^* + \bar{q} \to \bar{q} + g$, and $\gamma^* + g \to q + \bar{q}$ contribute to the two-jet cross section. At $\mathcal{O}(\alpha_s^2)$ the real emission corrections involve $\gamma^* + q \to q + g + g$, $\gamma^* + q \to q + \bar{q} + q$, $\gamma^* + g \to q + \bar{q} + g$ and analogous anti-quark initiated processes. The corresponding cross sections are calculated by numerically evaluating the tree level helicity amplitudes as given in Ref. [8]. The tree level matrix elements are numerically checked against the matrix elements in [9,10]. They need to be integrated over the entire phase space, including the unresolved regions, where only two jets are reconstructed according to a given jet definition scheme. In order to isolate the infrared as well as collinear divergencies associated with these unresolved regions the resolution parameter s_{min} is introduced. This s_{min} technique has already been successfully applied to next-to-leading order calculations of jet cross sections in e^+e^- annihilation and in hadronic collisions [11,12]. Soft and collinear approximations are used in the region where at least one pair of partons, including initial ones, has $s_{ij} = 2p_i \cdot p_j < s_{min}$ and the soft and/or collinear final state parton is integrated over analytically. Factorizing the collinear initial state divergencies into the bare parton distribution functions and adding this soft+collinear part to the $\mathcal{O}(\alpha_s^2)$ virtual contributions for the $\gamma^* + q \to q + g$, $\gamma^* + \bar{q} \to \bar{q} + g$, and $\gamma^* + g \to q + \bar{q}$ subprocesses gives a finite result for, effectively, 2-parton final states. In general this 2-parton contribution is negative and grows logarithmically in magnitude as s_{min} is decreased. This logarithmic growth is exactly cancelled by the increase in the 3 parton cross section, once s_{min} is small enough for the approximations to be valid.

As mentioned before the collinear initial state divergencies are factorized into the bare parton densities introducing a dependence on the factorization scale μ_F. In order to handle these singularities we follow Ref. [12] and use the technique of universal "crossing functions".

The integration over the 3-parton phase space with $s_{ij} > s_{min}$ is done by Monte-Carlo techniques (without using any approximations). In general, s_{min} has to be chosen fairly small (below ≤ 0.1 GeV^2). Therefore, the effective 2-parton final state (soft+collinear+virtual part) does not depend on the recombination scheme. The essential benefit of the Monte

Carlo approach in MEPJET is that all hard phase space integrals over the region $s_{ij} > s_{min}$ are performed numerically. Since, at each phase space point, the parton 4-momenta are available, the program is flexible enough to implement arbitrary jet algorithms and kinematical resolution and acceptance cuts.

For the numerical studies below, the standard set of parton distribution functions is MRS set D-' [13]. We employ the two loop formula for the strong coupling constant with $\Lambda^{(4)}_{\overline{MS}} = 230$ MeV, which is the value from the parton distribution functions. The value of α_s is matched at the thresholds $\mu_R = m_q$ and the number of flavors is fixed to $n_f = 5$ throughout, *i.e.* gluons are allowed to split into five flavors of massless quarks. Unless stated otherwise, the renormalization scale and the factorization scale are set to $\mu_R = \mu_F = 1/2 \sum_i p_T^B(i)$, where $p_T^B(i)$ denotes the magnitude of the transverse momentum of parton i in the Breit frame. A running QED fine structure constant $\alpha(Q^2)$ is used. The lepton and hadron beam energies are 27.5 and 820 GeV, respectively. A minimal set of kinematical cuts is imposed on the initial virtual photon and on the final state electron and jets. We require 40 GeV$^2 < Q^2 < 2500$ GeV^2, $0.04 < y < 1$, an energy cut of $E(e') > 10$ GeV on the scattered electron, and a cut on the pseudo-rapidity $\eta = -\ln\tan(\theta/2)$ of the scattered lepton and jets of $|\eta| < 3.5$. In addition jets must have transverse momenta of at least 2 GeV in both the lab and the Breit frame.

Within these general cuts four different jet definition schemes are considered for which we have chosen parameters such as to give similar LO cross sections. Note however, that the phase space region for the accepted dijet events depends on the jetalgorithm and thus somewhat different event sets would be considered in an actual experiment. Unless stated otherwise, and for all jet algorithms, we use the E-scheme to recombine partons, i.e. the cluster momentum is taken as $p_i + p_j$, the sum of the 4-momenta of partons i and j, if these are unresolved according to a given jet definition scheme.

1) W-scheme:
In the W-scheme the invariant mass squared, $s_{ij} = (p_i + p_j)^2$, is calculated for each pair of final state particles (including the proton remnant) [9]. If the pair with the smallest invariant mass squared is below $y_{cut} W^2$, the pair is clustered according to a recombination scheme. This process is repeated until all invariant masses are above $y_{cut} W^2$. The resolution parameter y_{cut} is fixed to 0.02.

2) JADE-scheme:
The experimental analyses in [1] are based on a variant of the W-scheme, the "JADE" algorithm [14]. It is obtained from the W-scheme by replacing the invariant definition $s_{ij} = (p_i + p_j)^2$ by $M_{ij}^2 = 2E_iE_j(1 - \cos\theta_{ij})$, where all quantities are defined in the laboratory frame. Neglecting the explicit mass terms p_i^2 and p_j^2 in the definition of M_{ij}^2 causes substantial differences in jet cross sections between the W and the JADE scheme.

3) cone scheme:
In the cone algorithm (which is defined in the laboratory frame) the distance $\Delta R = \sqrt{(\Delta\eta)^2 + (\Delta\phi)^2}$ between two partons decides whether they should be recombined to a single jet. Here the variables are the pseudo-rapidity η and the azimuthal angle ϕ. We recombine partons with $\Delta R < 1$. Furthermore, a cut on the jet transverse momenta

of $p_T(j) > 5$ GeV in the lab frame is imposed in addition to the 2 GeV Breit frame cut.

4) k_T scheme:
For the k_T algorithm (which is implemented in the Breit frame), we follow the description introduced in Ref. [15]. The hard scattering scale E_T^2 is fixed to 40 GeV^2 and $y_{cut} = 1$ is the resolution parameter for resolving the macro-jets. In addition, jets are required to have a minimal transverse momentum of 5 GeV in the Breit frame.

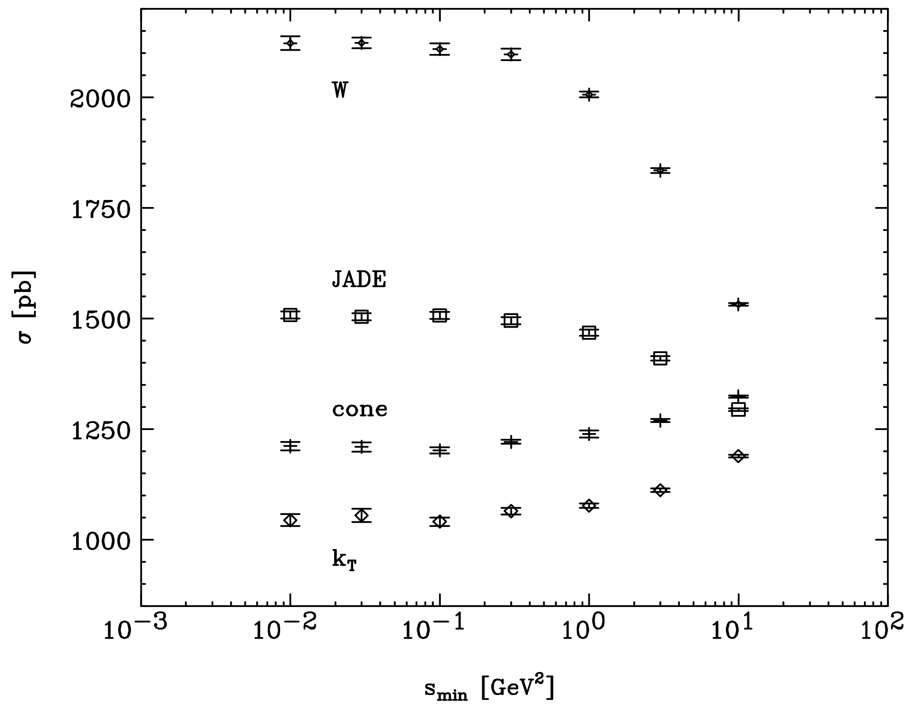

FIG. 1. Dependence of the inclusive two-jet cross section in the k_T, cone, JADE, and the W-scheme on s_{min}, the two-parton resolution parameter. Partons are recombined in the E-scheme. Error bars represent statistical errors of the Monte Carlo program. For the fairly soft jet definition criteria described in the text, s_{min} independence is achieved for $s_{min} \lesssim 0.1$ GeV^2.

A powerful test of the numerical program is the s_{min} independence of the NLO two jet cross sections for all jet algorithms. Fig. 1 shows the inclusive dijet cross section as a function of s_{min} for the four jet algorithms. As mentioned before, s_{min} is an arbitrary theoretical parameter and any measurable quantity should not depend on it. One observes that for values smaller than 0.1 GeV^2 the results are indeed independent of s_{min}. The strong s_{min} dependence of the NLO cross sections for larger values shows that the soft and collinear approximations used in the phase space region $s_{ij} < s_{min}$ are no longer valid, *i.e.* terms of $\mathcal{O}(s_{min})$ and $\mathcal{O}(s_{min} \ln s_{min})$ become important. In general, one wants to choose s_{min} as large as possible to avoid large cancellations between the virtual+collinear+soft part ($s_{ij} < s_{min}$) and the hard part of the phase space ($s_{ij} > s_{min}$). Note that factor 10 cancellations occur between the effective 2-parton and 3-parton final states at the lowest s_{min} values in Fig. 1

and hence very high Monte Carlo statistics is required for these points. s_{min} independence is achieved at and below $s_{min} = 0.1$ GeV^2 and we choose this value for our further studies.

III. DIJET CROSS SECTIONS IN NLO

A. K-Factors and Recombination Scheme Dependence

Table I shows the importance of higher order corrections and recombination scheme dependencies [16] of the two jet cross sections for the four jet algorithms. While the higher order corrections and recombination scheme dependencies in the cone and k_T schemes are small, very large corrections appear in the W-scheme. In addition, the large effective K-factor (defined as $K = \sigma_{NLO}/\sigma_{LO}$) of 2.04 (2.02) for the two-jet inclusive (exclusive) cross section in the W-scheme depends strongly on the recombination scheme which is used in the clustering algorithm. Such large dependencies are subject to potentially large higher order uncertainties, since the recombination dependence is only simulated at tree level in the NLO calculation.

The large corrections and recombination scheme dependencies in particular in the W scheme can partly be traced to large single jet masses (compared to their energy in the parton center of mass frame). As has been shown in [2], 50 % of the events in the NLO cross section for the W scheme (with the E recombination scheme) have a massive jet with $m/E > 0.44$, while substantially smaller values are found in the other jet schemes. The very large median value of m/E in the W-scheme implies that at NLO we are dealing with very different types of jets than at LO, and this difference accounts for the large K-factor.

In the JADE-algorithm the K-factor is reduced from 1.48 in the E-scheme to 1.36 and 1.24 in the $E0$ and P-schemes[2]. For the cone (k_T) scheme this recombination scheme dependence is reduced to the 3% (10%) level.

TABLE I. Two-jet cross sections in DIS at HERA. Results are given at LO and NLO for the four jet definition schemes and acceptance cuts described in the text. The 2-jet inclusive cross section at NLO is given for three different recombination schemes.

	2-jet LO	2-jet exclusive NLO (E)	2-jet inclusive NLO (E)	2-jet inclusive NLO ($E0$)	2-jet inclusive NLO (P)
cone	1107 pb	1047 pb	1203 pb	1232 pb	1208 pb
k_T	1067 pb	946 pb	1038 pb	1014 pb	944 pb
W	1020 pb	2061 pb	2082 pb	1438 pb	1315 pb
JADE	1020 pb	1473 pb	1507 pb	1387 pb	1265 pb

[2]The NLO two jet cross sections for the W or the JADE scheme in Table I disagree with previous calculations [17]. The DISJET program [10], for example, gives a K-factor very close to unity for a phase space region which is very similar.

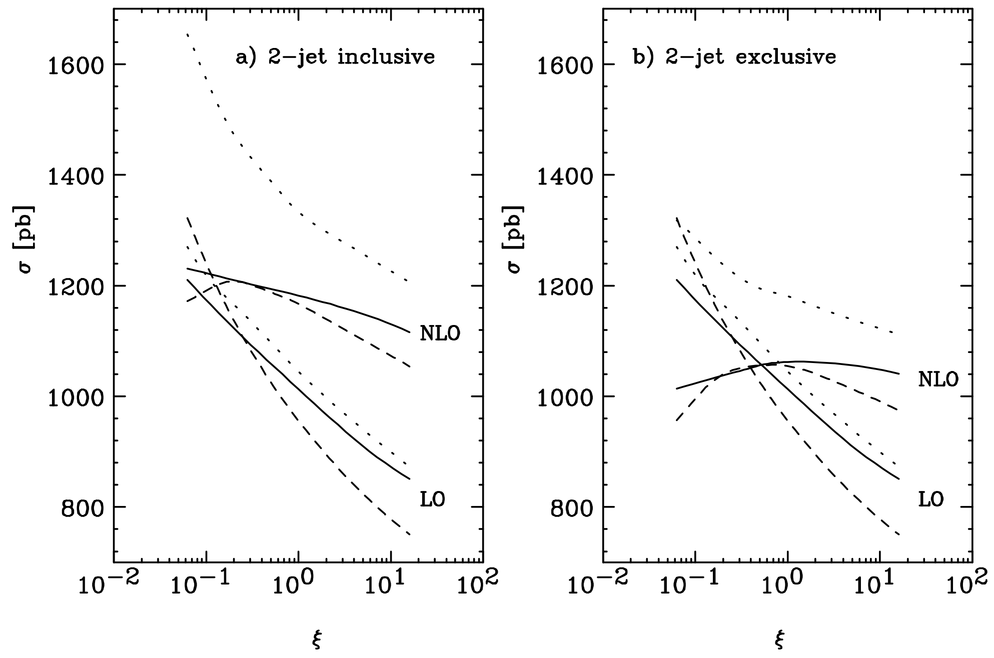

FIG. 2. Dependence of a) the two-jet inclusive and b) the two-jet exclusive cross section in the cone scheme on the renormalization and factorization scale factor ξ. The solid curves are for $\mu_R^2 = \mu_F^2 = \xi\ (\sum_i\ p_T^B(i))^2$, while for the dashed curves only $\xi_R = \xi$ is varied but $\xi_F = 1/4$ is fixed. Choosing the photon virtuality as the basic scale yields the dotted curves, which correspond to $\mu_R^2 = \mu_F^2 = \xi\ Q^2$. Results are shown for the LO (lower curves) and NLO calculations.

B. Scale Dependence

As mentioned before, the NLO corrections substantially reduce the the renormalization and factorization scale dependence which is present in the LO calculations and thus reliable cross section predictions in terms of $\alpha_s(m_Z)$ are made possible. The scale dependence for dijet cross sections in the cone scheme is shown in Fig. 2. We have considered scales related to the scalar sum of the parton transverse momenta in the Breit frame, $\sum_i\ p_T^B(i)$, and the virtuality Q^2 of the incident photon. In Fig. 2 the dependence of the two-jet cross section, in the cone scheme, on the renormalization and factorization scale factors ξ_R and ξ_F is shown. For scales related to $\sum_i\ p_T^B(i)$ they are defined via

$$\mu_R^2 = \xi_R\ (\sum_i\ p_T^B(i))^2\,, \qquad \mu_F^2 = \xi_F\ (\sum_i\ p_T^B(i))^2\,. \tag{1}$$

For the two-jet inclusive cross section of Fig. 2a, the LO variation by a factor 1.43 is reduced to a 10% variation at NLO when both scales are varied simultaneously over the plotted range (solid curves). However, neither the LO nor the NLO curves show an extremum. The uncertainty from the variation of both scales for the NLO two-jet exclusive cross section in Fig. 2b (solid curves) is reduced to 5%. Furthermore, the two-jet exclusive cross section now has a maximum and is equal to the LO cross section for $\xi = 0.5$. Also shown is the $\xi = \xi_R$ dependence of LO and NLO cross sections at fixed $\xi_F = 1/4$ (dashed curves). In this case a maximum appears in the NLO inclusive and exclusive cross sections. However, the scale variation is stronger than in the $\xi = \xi_R = \xi_F$ case.

An alternative scale choice might be $\mu_R^2 = \mu_F^2 = \xi\, Q^2$. The resulting ξ dependence is shown as the dotted lines for both the LO and NLO calculations. At LO the two scale choices give qualitatively similar results. However, with $\mu_R^2 = \mu_F^2 = \xi\, Q^2$, the scale dependence does not markedly improve at NLO. We therefore use the jet transverse momenta in the Breit frame to set the scale and fix $\xi_R = \xi_F = 1/4$ in Eq. (1) for the following numerical results. A careful study of the scale dependence and the choice of the scale in the dijet cross section is needed in order to extract a reliable value for $\alpha_s(M_z)$.

IV. GLUON DENSITY DETERMINATION

HERA opens a new window to measure the proton structure functions, in particular the gluon distribution, in a completely new kinematic region. The accessible range in the Bjorken-scaling variable x can be extended considerably towards low x compared to previous fixed target experiments. Dijet production in DIS at HERA in principle allows for a more direct measurement of the gluon density in the proton (via $\gamma g \to q\bar{q}$) than an analysis of the structure function F_2.

For these studies we use the cone scheme as defined in section II. The Q^2 range is lowered to $5 < Q^2 < 2500$ GeV^2 and the cut on the jet transverse momenta in the Breit frame is increased to 5 GeV. The LO (NLO) results are based on the LO (NLO) parton distributions from GRV [18] together with the one-loop (two-loop) formula for the strong coupling constant. With these parameters, one obtains 2890 pb (2846 pb) for the LO (NLO) two jet exclusive cross section.

In order to investigate the feasibility of the parton density determination at low x, Fig. 3a shows the Bjorken x distribution of the two jet exclusive cross section in the cone scheme. The gluon initiated subprocess clearly dominates the Compton process for small x in the LO predictions. The effective K-factor close to unity for the total exclusive dijet cross section is a consequence of compensating effects in the low x ($K > 1$) and high x ($K <1$) regime.

For the isolation of parton structure functions we are interested in the fractional momentum x_i of incoming parton i ($i = q, g$), however, and in dijet production x and x_i differ substantially. Denoting as s_{jj} the invariant mass squared of the produced dijet system, and considering two-jet exclusive events only, the two are related by

$$x_i = x\,\left(1 + \frac{s_{jj}}{Q^2}\right) \tag{2}$$

The s_{jj} distribution of Fig. 3b exhibits rather large NLO corrections as well. The invariant mass squared of the two jets is considerable larger at NLO than at LO (the mean value of s_{jj} rising to 570 GeV^2 at NLO from 470 GeV^2 at LO).

The NLO corrections to the x and s_{jj} distributions have a compensating effect on the x_i distribution in Fig. 3c, which shows very similar shapes at LO and NLO. At LO a direct determination of the gluon density is possible from this distribution, after substraction of the calculated Compton subprocess. This simple picture is modified in NLO, however, and the effects of Altarelli-Parisi splitting and low p_T partons need to be taken into account more

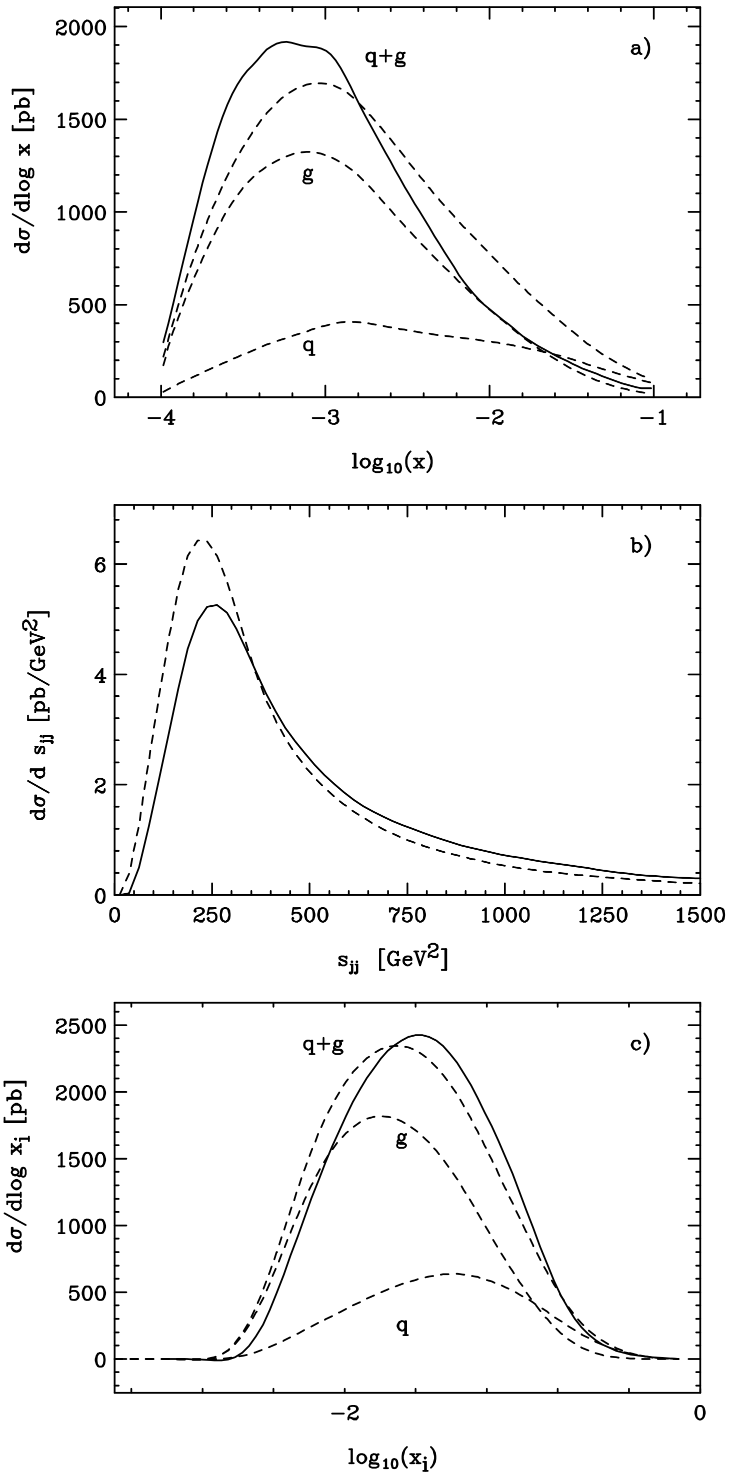

FIG. 3. a) Dependence of the exclusive two-jet cross section in the cone scheme on Bjorken x for the quark and gluon initiated subprocesses and for the sum. Both LO (dashed) and NLO (solid) results are shown; b) Dijet invariant mass distribution in LO (dashed) and in NLO (solid); c) Same as a) for the x_i distribution, x_i representing the momentum fraction of the incident parton at LO.

TABLE II. Forward jet cross sections in [pb] in DIS at HERA.

	with forward jet	without forward jet	relative phase space
1 jet (LO)	0 pb	9026 pb	0%
2 jet (LO)	19.3 pb	2219 pb	0.87%
2 jet (NLO)	68 pb	2604 pb	2.61%
3 jet (LO)	30.1 pb	450 pb	6.7%

carefully to determine the structure functions at a well defined factorization scale μ_F. We will further investigate this problem in a subsequent publication. One method to determine the gluon density in NLO is presented in [19].

V. FORWARD JET PRODUCTION IN THE LOW X REGIME

Deep inelastic scattering with a measured forward jet with relatively large momentum fraction x_{jet} (in the proton direction) and $p_T^{2\,lab}(j) \approx Q^2$ is expected to provide sensitive information about the BFKL dynamics at low x [20,21]. In this region there is not much phase space for DGLAP evolution with transverse momentum ordering, whereas large effects are expected for BFKL evolution in x. In particular, BFKL evolution is expected to substantially enhance cross sections in the region $x << x_{jet}$ [20,21]. In order to extract information on the $\ln(1/x)$ BFKL evolution, one needs to show that cross section results based on fixed order QCD with DGLAP evolution are not sufficient to describe the data. Clearly, next-to-leading order QCD corrections to the DGLAP predictions are needed to make this comparison between experiment and theory.

In Table II we show numerical results for the multi jet cross sections with (or without) a forward jet. The LO (NLO) results are based on the LO (NLO) parton distributions from GRV [18] together with the one-loop (two-loop) formula for the strong coupling constant. Kinematical cuts are imposed to closely model the H1 event selection [22]. More specifically, we require $Q^2 > 8$ GeV^2 , $x < 0.004$, $0.1 < y < 1$, an energy cut of $E(e') > 11$ GeV on the scattered electron, and a cut on the pseudo-rapidity $\eta = -\ln\tan(\theta/2)$ of the scattered lepton of $-2.868 < \eta(e') < -1.735$ (corresponding to $160^o < \theta(l') < 173.5^o$). Jets are defined in the cone scheme (in the laboratory frame) with $\Delta R = 1$ and $|\eta(j)| < 3.5$. We require a forward jet with $x_{jet} = p_z(j)/E_P > 0.05$, $E(j) > 25$ GeV, $0.5 < p_T^2(j)/Q^2 < 4$, and a cut on the pseudo-rapidity of $1.735 < \eta(j) < 2.9$ (corresponding to $6.3^o < \theta(j) < 20^o$). In addition all jets must have transverse momenta of at least 4 GeV in the lab frame and 2 GeV in the Breit frame.

The cross sections of Table II demonstrate first of all that the requirement of a forward jet with large longitudinal momentum fraction ($x_{jet} > 0.05$) and restricted transverse momentum ($0.5 < p_T^2(j)/Q^2 < 4$) severely restricts the available phase space, in particular for low jet multiplicities. The 1-jet exclusive cross section vanishes at LO, due to the contradicting $x < 0.004$ and $x_{jet} > 0.05$ requirements. For $x << x_{jet}$, a high invariant mass hadronic system must be produced by the photon-parton collision and this condition translates into

$$2E(j)m_T\, e^{-y} \approx \hat{s}_{\gamma,parton} \approx Q^2\left(\frac{x_{jet}}{x}-1\right) >> Q^2\,, \tag{3}$$

where m_T and y are the transverse mass and rapidity of the partonic recoil system, respectively. Thus a recoil system with substantial transverse momentum and/or invariant mass must be produced and this condition favors recoil systems composed out of at least two additional energetic partons.

As a result one finds very large fixed order perturbative QCD corrections (compare 2 jet LO and NLO results with a forward jet in Table II). In addition, the LO ($\mathcal{O}(\alpha_s^2)$) 3-jet cross section is larger than the LO ($\mathcal{O}(\alpha_s)$) 2-jet cross section. Thus, the forward jet cross sections in Table II are dominated by the ($\mathcal{O}(\alpha_s^2)$) matrix elements. The effects of BFKL evolution must be seen and isolated on top of these fixed order QCD effects. We will analyze these effects in a subsequent publication.

VI. CONCLUSIONS

The calculation of NLO perturbative QCD corrections has received an enormous boost with the advent of full NLO Monte Carlo programs [11,12,23]. For dijet production at HERA the NLO Monte Carlo program MEPJET [2] allows to study jet cross sections for arbitrary jetalgorithms. Internal jet structure, parton/hadron recombination effects, and the effects of arbitrary acceptance cuts can now be simulated at the full $\mathcal{O}(\alpha_s^2)$ level. We found large NLO effects for some jet definition schemes (in particular the W-scheme) and cone and k_T schemes appear better suited for precision QCD tests.

The extraction of gluon distribution functions is now supported by a fully versatile NLO program. Preliminary studies show that large NLO corrections are present in the Bjorken x distribution for dijet events, while these effects are mitigated in the reconstructed Feynman x (x_i) distribution, thus aiding the reliable extraction of $g(x_i, \mu_F^2)$.

For the study of BFKL evolution by considering events with a forward "Mueller"-jet very large QCD corrections are found at $\mathcal{O}(\alpha_s^2)$. These fixed order effects form an important background to the observation of BFKL evolution at HERA. They can now be studied systematically and for arbitrary jetalgorithms.

ACKNOWLEDGMENTS

This research was supported by the University of Wisconsin Research Committee with funds granted by the Wisconsin Alumni Research Foundation and by the U. S. Department of Energy under Grant No. DE-FG02-95ER40896. The work of E. M. was supported in part by DFG Contract Ku 502/5-1.

REFERENCES

[1] H1 Collaboration, T. Ahmed et. al., Phys. Lett. **B346** (1995) 415;
ZEUS Collaboration, M. Derrick et al., Phys. Lett. **B363** (1995) 201.

[2] E. Mirkes and D. Zeppenfeld, TTP95-42, MADPH-95-916, (1995), hep-ph/9511448.

[3] ZEUS Collaboration, M. Derrick et al., Z. Phys. **C65** (1995) 379;
ibid. Phys. Lett. **B345** (1995) 576;
H1 Collaboration, T. Ahmed et. al., Nucl. Phys. **B439** (1995) 471;
ibid. Phys. Lett. **B354** (1995) 494.

[4] H1 Collaboration, T. Ahmed et. al., Nucl. Phys. **B449** (1995) 3.

[5] E.A. Kuraev, L.N. Lipatov and V.S. Fadin, **JETP 45** (1972) 199;
Y.Y. Balitsky and L.N. Lipatov, Sov. J. Nucl. Phys. **28** (1978) 282.

[6] G. Altarelli and G. Parisi, Nucl. Phys. **126** (1977) 297;
V.N. Gribov and L.N. Lipatov, Sov. J. Nucl. Phys. **15** (1972) 438 and 675;
Yu. L. Dokshitzer, Sov. Phys. **JETP 46** (1977) 641.

[7] C. Ziegler and E. Mirkes, Nucl. Phys. **B429** (1994) 93; and references therein.

[8] K. Hagiwara and D. Zeppenfeld, Nucl. Phys. **B313** (1989) 560.

[9] J.G. Körner, E. Mirkes and G. Schuler, Int. J. Mod. Phys. **A4** (1989) 1781;
T. Brodkorb, J.G. Körner, E. Mirkes, and G. Schuler, Z. Phys. **C44** (1989) 415.

[10] T. Brodkorb and E. Mirkes, Madison preprint, MAD/PH/821 (1994).

[11] W. T. Giele and E. W. N. Glover, Phys. Rev. D **46** (1992) 1980.

[12] W. T. Giele, E. W. N. Glover and D.A. Kosower, Nucl. Phys. **B403** (1993) 633.

[13] A.D. Martin, W.J. Stirling and R.G. Roberts, Phys. Lett. **B306** (1993) 145.

[14] JADE Collaboration, W. Bartel et al. Z. Phys. **C33** (1986) 23.

[15] S. Catani, Y.L. Dokshitzer and B.R. Webber, Phys. Lett. **B285** (1992) 291.

[16] For the definition of the recombination schemes see, for example,
S. Bethke, Z. Kunszt, D.E. Soper and W.J. Stirling, Nucl. Phys. **B370** (1992) 310.

[17] T. Brodkorb and J.G. Körner, Z. Phys. **C54** (1992) 519;
D. Graudenz, Phys. Lett. **B256** (1992) 518; Phys. Rev. **D49** (1994) 3291;
T. Brodkorb and E. Mirkes, Z. Phys. **C66** (1995) 141.

[18] M. Glück, E. Reya and A. Vogt, Z. Phys. **C67** (1995) 433.

[19] D. Graudenz, M. Hampel, A. Vogt, C. Berger, CERN-TH-95-149, (1995).

[20] A.H. Mueller, Nucl. Phys. **B** (Proc. Suppl.) **18C** (1990) 125; J. Phys. **G17** (1991) 1443.

[21] J. Kwiecinski, A.D. Martin and P.J. Sutton, Phys. Rev. **D46** (1992) 921;
J. Bartels, A. De Roeck and M. Loewe, Z. Phys. **C54** (1992) 635;
W.K. Tang, Phys. Lett. **B278** (1992) 363.

[22] The cuts are similar to the cuts used in the present H1 forward jet analyses. We thank A. De Roeck and E.M. Mroczko for this information.

[23] H. Baer, J. Ohnemus, and J. F. Owens, Phys. Rev. **D40** (1989) 2844; Phys. Lett. **B234** (1990) 127; Phys. Rev. **D42** (1990) 61.